Composites: Part B 58 (2014) 318–327

Contents lists available at ScienceDirect

Composites: Part B

journal homepage: www.elsevier.com/locate/compositesb

Mechanical properties of hybrid composites using finite element method based micromechanics

Sayan Banerjee *, Bhavani V. Sankar

Department of Mechanical and Aerospace Engineering, University of Florida, Gainesville, FL 32608-6250, USA

ARTICLE INFO

Article history:
Received 18 April 2013
Received in revised form 16 September 2013
Accepted 25 October 2013
Available online 7 November 2013

Keywords:
A. Hybrid
B. Mechanical properties
C. Finite element analysis (FEA)
C. Micro-mechanics

ABSTRACT

A micromechanical analysis of the representative volume element of a unidirectional hybrid composite is performed using finite element method. The fibers are assumed to be circular and packed in a hexagonal array. The effects of volume fractions of the two different fibers used and also their relative locations within the unit cell are studied. Analytical results are obtained for all the elastic constants. Modified Halpin–Tsai equations are proposed for predicting the transverse and shear moduli of hybrid composites. Variability in mechanical properties due to different locations of the two fibers for the same volume fractions was studied. It is found that the variability in elastic constants and longitudinal strength properties was negligible. However, there was significant variability in the transverse strength properties. The results for hybrid composites are compared with single fiber composites.

1. Introduction

Hybrid composites contain more than one type of fiber in a single matrix material. In principle, several different fiber types may be incorporated into a hybrid, but it is more likely that a combination of only two types of fibers would be most beneficial [1]. They have been developed as a logical sequel to conventional composites containing one fiber. Hybrid composites have unique features that can be used to meet various design requirements in a more economical way than conventional composites. This is because expensive fibers like graphite and boron can be partially replaced by less expensive fibers such as glass and Kevlar [2]. Some of the specific advantages of hybrid composites over conventional composites include balanced effective properties, reduced weight and/or cost, with improvement in fatigue and impact properties [1].

Experimental techniques can be employed to understand the effects of various fibers, their volume fractions and matrix properties in hybrid composites. However, these experiments require fabrication of various composites which are time consuming and cost prohibitive. Advances in computational micromechanics allow us to study the various hybrid systems by using finite element simulations and it is the goal of this paper.

Hybrid composites have been studied for more than 30 years. Numerous experimental works have been conducted to study the effect of hybridization on the effective properties of the composite [3–11]. The mechanical properties of hybrid short fiber composites can be evaluated using the rule of hybrid mixtures (RoHM) equation, which is widely used to predict the strength and modulus of hybrid composites [3]. It is shown however, that RoHM works best for longitudinal modulus of the hybrid composites. Since, elastic constants of a composite are volume averaged over the constituent microphases, the overall stiffness for a given fiber volume fraction is not affected much by the variability in fiber location. The strength values on the other hand are not only functions of strength of the constituents; they are also very much dependent on the fiber/matrix interaction and interface quality. In tensile test, any minor (microscopic) imperfection on the specimen may lead to stress build-up and failure could not be predicted directly by RoHM equations [12].

The computational model presented in this paper considers random fiber location inside a representative volume element for a given volume fraction ratio of fibers, in this case, carbon and glass. The variability in fiber location seems to have considerable effect on the transverse strength of the hybrid composites. For the transverse stiffness and shear moduli, a semi-empirical relation similar to Halpin–Tsai equations has been derived. Direct Micromechanics Method (DMM) is used for predicting strength, which is based on first element failure method; although conservative, it provides a good estimate for failure initiation [13].

1.1. Model for hybrid composite

The fiber orientation depends on processing conditions and may vary from random in-plane and partially aligned to approximately

* Corresponding author. Tel.: +1 6175849862.
E-mail addresses: sbanerjee@ufl.edu (S. Banerjee), sankar@ufl.edu (B.V. Sankar).

1359-8368/$ - see front matter © 2013 Elsevier Ltd. All rights reserved.
http://dx.doi.org/10.1016/j.compositesb.2013.10.065

uniaxial [1]. The fiber packing arrangement, for most composites, is random in nature, so that the properties are approximately same in any direction perpendicular to the fiber (i.e. properties along the 2-direction and 3-direction are same, and is invariant with rotations about the 1-axis), resulting in transverse isotropy [14]. For this paper, it is assumed that the fibers are arranged in a hexagonal pattern and the epoxy matrix fills up the remaining space in the representative volume element (RVE). Hexagonal pattern was selected because it can more accurately represent transverse isotropy as compared to a square arrangement. The RVE consists of 50 fibers. Multiple fibers were selected to allow randomization of fiber location. Hybrid composites are created by varying the number of fibers of carbon and glass to obtain hybrid composites of different volume fractions.

A cross section of a hybrid composite of polypropylene reinforced with short glass and carbon fibers is shown in Fig. 1 [3]. The black circles represent glass fibers (V_{fg} 6.25%) and the white circles represent carbon fibers (V_{fc} 18.75%). In order to represent such an arrangement, we consider the schematic of the RVE as shown in Fig. 2. Green and red represent two different fiber materials, while the matrix is shown in white. Also, it is assumed that the radii of the fibers are the same and only the count of carbon and glass fibers vary. This gives us much more flexibility in creating the finite element mesh. Although, this RVE architecture is a lot simplistic and entails some basic assumptions like same size and location of the fibers and absence of voids but there is still a lot to earn from the parameters that have been used.

The properties of the composite are independent of the 1-direction, hence a 2D analysis is performed. We have assumed here that the fibers remain unidirectional with no fiber undulation and waviness. An overall fiber volume fraction of 60% is assumed for all the composites analyzed in this paper. The proportions of the reinforcements have been varied to obtain five hybrid composites, keeping the total volume fraction of reinforcement phases constant. The volume fraction of any particular reinforcement, say A, was determined by the relation

$$V_{f\mathrm{A}} = 0.6\left(\frac{N_{\mathrm{A}}}{N_T}\right) \tag{1}$$

where N is the number of fibers of reinforcement A and N_T is the total number of fibers. (see Table 1).

2. Analysis for elastic constants

The RVE of the composite is analyzed using commercially available finite element software (ABAQUS/CAE 6.9-2). The composite is assumed to be under a state of uniform strain at the macroscopic level called macroscale strains or macrostrains, and the corresponding stresses are called macrostresses. However, the microstresses, which are the actual stresses inside the RVE can have a spatial variation. The macrostresses are average stress required to produce a given state of macro-deformations, and they can be computed using finite element method. The macrostresses and macrostrain follow the relation

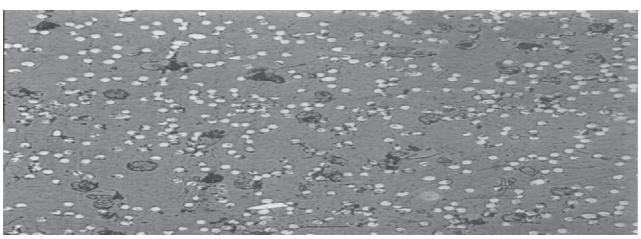

Fig. 1. Cross sectional area of a composite with V_{fc} 18.75% and V_{fg} (glass) = 6.25% [3].

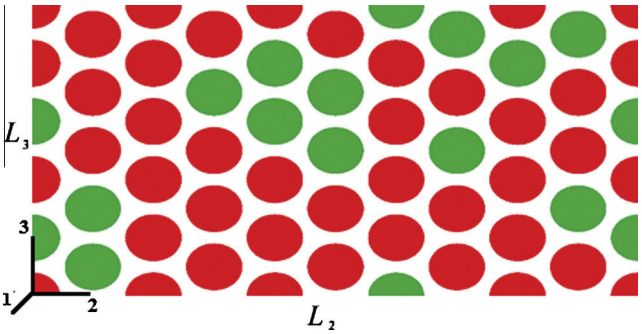

Fig. 2. RVE for Hybrid composite. fibers of two different reinforcements have different colors. (For interpretation of the references to colour in this figure legend, the reader is referred to the web version of this article.)

Table 1
Specimen numbering for the Hybrid Composites.

Specimen	V_{fc}	V_{fg}	V_f
H1	0.54	0.06	0.6
H2	0.42	0.18	0.6
H3	0.3	0.3	0.6
H4	0.18	0.42	0.6
H5	0.06	0.54	0.6

$$\{\sigma^M\} = [C]\{\varepsilon^M\} \tag{2}$$

where $[C]$ is the elastic constant of the homogenized composite, also known as the stiffness matrix. In this method, the RVE is subjected to six independent macrostrains. For each applied non-zero macrostrain, it is also subjected to periodic boundary conditions such that all other macrostrains are zero. The six cases are: Case 1: $\varepsilon_{11}^M = 1$; Case 2: $\varepsilon_{22}^M = 1$; Case 3: $\varepsilon_{33}^M = 1$; Case 4: $\gamma_{12}^M = 1$; Case 5: $\gamma_{13}^M = 1$; Case 6: $\gamma_{23}^M = 1$ [15], where the subscripts 1, 2, 3 are parallel to the material principal directions, as shown in Fig. 3, and the superscript M stands for macrostress or macrostrain.

2.1. Finite element analysis

For case 1, 2 and 4, a mixture of three and four-node plane strain elements, CPE3/CPE4 and for case 3, a mixture of three and four node generalized plane strain elements, CPEG3/CPEG4 were used. For cases 5 and 6 (longitudinal shear), three and four node shell elements were used, because out of plane displacements have to be applied for this case. Periodic boundary conditions (PBC) were applied on opposite faces of the RVE which are described in Table 2. Appropriate constraints on the RVE depend on the loading condition and have been determined by symmetry and periodicity conditions in [16]. For each strain case, six microstresses were calculated, three normal and three shear stresses in the 1-2-3 directions, in each element in the finite element model and volume averaged to find the macrostress for the RVE. The finite element model used is shown in Fig. 3, which contains 27,000 elements. The $[C]$ matrix can be inverted to obtain the compliance matrix or $[S]$ matrix, from which the elastic constants can be computed using the following relation

$$[C]^{-1} = [S] = \begin{bmatrix} \frac{1}{E_1} & \frac{-\nu_{12}}{E_1} & \frac{-\nu_{13}}{E_1} & 0 & 0 & 0 \\ \frac{-\nu_{21}}{E_2} & \frac{1}{E_2} & \frac{-\nu_{23}}{E_2} & 0 & 0 & 0 \\ \frac{-\nu_{31}}{E_3} & \frac{-\nu_{32}}{E_3} & \frac{1}{E_3} & 0 & 0 & 0 \\ 0 & 0 & 0 & \frac{1}{G_{23}} & 0 & 0 \\ 0 & 0 & 0 & 0 & \frac{1}{G_{13}} & 0 \\ 0 & 0 & 0 & 0 & 0 & \frac{1}{G_{12}} \end{bmatrix} \tag{3}$$

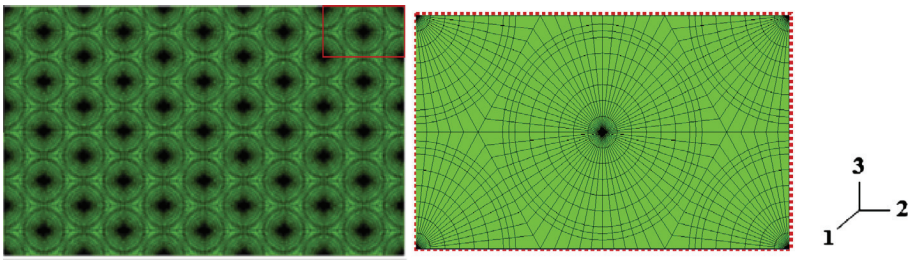

Fig. 3. Finite element model of the RVE and mesh of the repetitive block.

Table 2
Periodic boundary conditions for square unit cell. L_1, L_2 and the coordinate system is shown in Fig. 2.

Case	Constraint between left and right faces	Constraint between top and bottom faces	Out of plane strains
$\varepsilon_{11} = 1$	$u_i(L_2, x_3) - u_i(0, x_3) = 0$, $i = 2, 3$	$u_i(x_2, L_3) - u_i(x_2, 0) = 0$, $i = 2, 3$	$\varepsilon_{11} = 1$, $\gamma_{12} = 0$, $\gamma_{13} = 0$
$\varepsilon_{22} = 1$	$u_2(L_2, x_3) - u_2(0, x_3) = L_2$ $u_3(L_2, x_3) - u_3(0, x_3) = 0$	$u_2(x_2, L_3) - u_2(x_2, 0) = 0$ $u_3(x_2, L_3) - u_3(x_2, 0) = 0$	$\varepsilon_{11} = 0$, $\gamma_{12} = 0$, $\gamma_{13} = 0$
$\varepsilon_{33} = 1$	$u_2(L_2, x_3) - u_2(0, x_3) = 0$ $u_3(L_2, x_3) - u_3(0, x_3) = 0$	$u_2(x_2, L_3) - u_2(x_2, 0) = 0$ $u_3(x_2, L_3) - u_3(x_2, 0) = L_3$	$\varepsilon_{11} = 0$, $\gamma_{12} = 0$, $\gamma_{13} = 0$
$\gamma_{23} = 1$	$u_2(L_2, x_3) - u_2(0, x_3) = 0$ $u_3(L_2, x_3) - u_3(0, x_3) = L_2/2$	$u_2(x_2, L_3) - u_2(x_2, 0) = L_3/2$ $u_3(x_2, L_3) - u_3(x_2, 0) = 0$	$\varepsilon_{11} = 0$, $\gamma_{12} = 0$, $\gamma_{13} = 0$
$\gamma_{13} = 1$	$u_1(L_2, x_3) - u_1(0, x_3) = 0$ $u_2 = 0$; $u_3 = 0$, $u_{R1} = 0$, $u_{R2} = 0$; $u_{R3} = 0$ (for all nodes)	$u_1(x_2, L_3) - u_1(x_2, 0) = L_3$	$\varepsilon_{11} = 0$, $\gamma_{12} = 0$, $\gamma_{13} = 1$
$\gamma_{12} = 1$	$u_1(L_2, x_3) - u_1(0, x_3) = L_2$ $u_2 = 0$; $u_3 = 0$, $u_{R1} = 0$, $u_{R2} = 0$; $u_{R3} = 0$ (for all nodes)	$u_1(x_2, L_3) - u_1(x_2, 0) = 0$	$\varepsilon_{11} = 0$, $\gamma_{12} = 1$, $\gamma_{13} = 0$

In the above finite element model opposite faces of the RVE must have corresponding nodes for the periodic boundary conditions to be enforced using multi-point constraints. The material properties for the various constituents are listed in Table 3. For a composite to have transversely isotropic behavior in the 2–3 plane, it has to follow the relation

$$G_{23} = \frac{E_2}{2(1 + \nu_{23})} \tag{4}$$

As shown later in Table 8, all the composites including the hybrid composites studied in this paper closely follow transverse isotropic behavior. One reason for this may be the hexagonal packing of the fiber, which represents better isotropy in the 2–3 plane. As for the hybrid composites, 10 samples of each volume fraction ratio were considered, with the fiber locations randomly selected for each sample. The mean and standard deviation of the results were studied.

Rule of hybrid mixtures was used to predict the longitudinal modulus E_1 and the longitudinal Poisson's ratios, ν_{12} and ν_{13} for all the composites. For the transverse modulus E_2, and the shear moduli G_{12}, G_{13} and G_{23}, the Halpin–Tsai equation was modified to predict the results obtained from finite element method. As will be shown later the modified Halpin–Tsai equations agree with reasonable accuracy for the hybrid composites. For all the elastic constants, samples were generated with random fiber locations and results obtained for all the samples were studied to evaluate the effect of hybridization.

Table 3
Elastic constants of various constituents [17].

Property	E-glass fiber	Carbon fiber (IM7)	Epoxy
E_1 (GPa)	72.4	263	3.5
E_2, E_3 (GPa)	72.4	19	3.5
G_{12}, G_{13} (GPa)	30.2	27.6	1.29
G_{23} (GPa)	30.2	7.04	1.29
ν_{12}, ν_{13}	0.2	0.2	0.35
ν_{23}	0.2	0.35	0.35

3. Evaluation of strength properties

Failure is predicted using micromechanical failure analysis, which inspects every element in the finite element model for failure, also known as the Direct Micromechanics (DMM) approach to failure prediction. A flowchart that describes DMM can be found in [15]. Thus for a given state of macrostress, we need to calculate microstresses in every element in the RVE. The macrostrain for a given state of macrostress can be obtained from the constitutive relation for that composite using

$$\{\varepsilon^M\} = [C^{-1}]\{\sigma^M\} \tag{5}$$

From the unit cell analysis as discussed before, we have the microstresses in every element for six independent unit macrostrain cases. Thus, the microstresses for a given macrostress state can be obtained from principle of superposition as follows:

$$\{\sigma^{(e)}\} = [F^{(e)}]\{\varepsilon^M\} \tag{6}$$

where $\{\sigma^{(e)}\}$ is the microstress in Element e, and the matrix $[F^{(e)}]$ represents the microstresses in Element e for various states of unit macrostrains. For example, the first column in F_{ij} contains the six microstresses in Element e caused by unit macrostrain ε^M_{11}. However, in the present method it is assumed that there exist no thermal residual stresses in the material. Also, it is assumed that when the first element fails, the composite has failed.

It is assumed, that failure criteria for fibers and matrix phases are known. We have considered quadratic interaction failure criteria for carbon fiber which is the one proposed by Hashin for unidirectional fiber composites [18] and maximum principal stress failure criteria for glass fiber and epoxy.

4. Results and discussions

We have divided this section into two parts; one for the elastic constants and the other for the strength properties. Results obtained from analytical formulations, wherever applicable, have been compared with FEA results.

4.1. Elastic properties

The longitudinal modulus E_1 was calculated for the composites by varying the volume fraction of the reinforcements. It was observed that E_1 varies linearly with the variation of volume fraction. E_1 is plotted in Fig. 4 with the volume fraction of carbon varying from 0 to 0.6 as we move from left to right. E_1 for the composites are also tabulated in Table 4. Results obtained from the RoHM are also presented in the same table. The RoHM can be stated as

$$E_1 = E_{1c}V_{fc} + E_{1g}V_{fg} + E_mV_m \tag{7}$$

where E_{1c}, E_{1g} and E_m refers to the modulus values for carbon, glass and matrix respectively, and V_{fc}, V_{fg} and V_m refer to the volume fraction carbon, glass and matrix respectively. It can be seen that RoHM predicts the longitudinal moduli with very high accuracy.

The transverse modulus E_2 however, cannot be predicted accurately using equations of the form (7). A general method to estimate E_2 involves the use of semi-empirical equations such as the Halpin–Tsai equation that are adjusted to match experimental results. The Halpin–Tsai equation for single fiber composite is [14]

$$\frac{E_2}{E_m} = \frac{1+\xi\eta V_f}{1-\eta V_f} \tag{8}$$

where

$$\eta = ((E_f/E_m)+1)/((E_f/E_m)+\xi)$$

In the equations above, ξ is a curve-fitting parameter, which is dependent on the fiber packing arrangement. For the hybrid composites, we propose a modification to the Halpin–Tsai Eq. (8), which incorporates the volume fractions of all the reinforcements as follows:

$$\frac{E_2}{E_m} = \frac{1+\xi(\eta_c V_{fc} + \eta_g V_{fg})}{1-(\eta_c V_{fc} + \eta_g V_{fg})} \tag{9}$$

where,

$$\eta_c = ((E_{fc}/E_m)-1)/((E_{fc}/E_m)+\xi) \text{ and}$$
$$\eta_g = ((E_{fg}/E_m)-1)/((E_{fg}/E_m)+\xi)$$

Here the subscripts 'c' and 'g' refer to carbon and glass respectively. The optimum value of ξ was determined using a least square error procedure. It was found that ξ = 1.165 yielded the best results for E_2 including single fiber composites.

In Table 5 we have the E_2 values computed from both the finite element analysis and modified Halpin–Tsai equation. We see that (9) does a good job of predicting the transverse modulus of the composites. The variation of E_2 with increasing volume fraction of carbon is shown in Fig. 5.

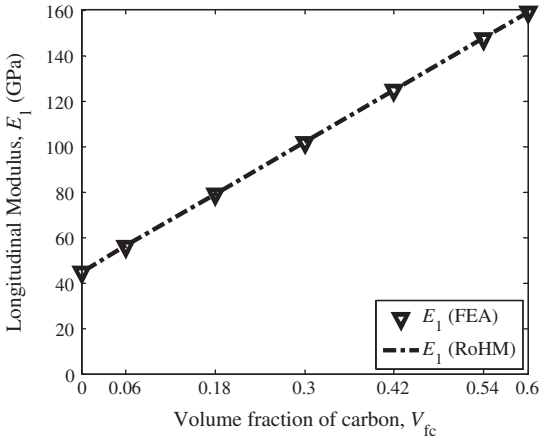

Fig. 4. Variation of E_1 with volume fraction of carbon.

The poissons' ratio v_{12} and v_{13} were computed for all composites and they were nearly equal for all cases. It was found that these two Poisson's ratios had a linear variation when volume fraction of carbon was gradually increased, as seen in Fig. 6. The RoHM for Poisson's ratios can be stated as

$$v_{12} = v_{12fc}V_{fc} + v_{12fg}V_{fg} + v_mV_m \tag{10}$$

Once again RoHM provides a good prediction of Poisson's ratio, where the Poisson's ratio of the composite, v_{12} can be found out using (10), where v_{12fc}, v_{12fg}, v_m refers to the Poisson's ratio of carbon, glass and matrix respectively.

A approach similar to the transverse modulus was considered for predicting the shear moduli, G_{12}, G_{13} and G_{23}. The modified Halpin–Tsai relation for predicting the shear moduli is as shown below:

$$\frac{G}{G_m} = \frac{1+\xi(\eta_c V_{fc} + \eta_g V_{fg})}{1-(\eta_c V_{fc} + \eta_g V_{fg})} \tag{11}$$

where,

$$\eta_c = ((G_{fc}/G_m)-1)/((G_{fc}/G_m)+\xi) \text{ and}$$
$$\eta_g = ((G_{fg}/G_m)-1)/((G_{fg}/G_m)+\xi)$$

In the above equation G refers to composite shear modulus (G_{12}, G_{13} or G_{23}). For each case, the corresponding fiber shear moduli have to be considered in calculating the parameter η. The optimal value of ξ was found out to be 1.01 for G_{12} and G_{13}, and 0.9 for G_{23}. The corresponding plots for variation of the three shear moduli with volume fraction of carbon are shown in Figs. 7 and 8. The moduli values calculated using modified Halpin–Tsai equation and the finite element analysis are also presented in Tables 6 and 7.

Poisson's ratio v_{23} is calculated and variation with changes in reinforcement volume fraction is studied. An analytical expression for v_{23} is not required, since for transverse isotropic composites v_{23} can be calculated from G_{23} and E_2. Since, we have an analytical expression for predicting E_2 and G_{23}, we can predict v_{23} once we have the other two material properties. The variation of v_{23} with volume fraction of carbon is as shown in Fig. 9.

As mentioned before, 10 random fiber locations inside the RVE were selected for each volume fraction for the hybrid composites. It was observed that none of the elastic constants showed significant variability with fiber location. The Poisson's ratio v_{23} had some variability, as shown in Fig. 9 but it was observed that the coefficient of variation for all the elastic constants were negligibly small. This can be attributed to the fact that elastic constants were calculated by volume averaging the microstresses for all the elements. Hence, the spatial variation of the microstresses does not have significant effect on the elastic constants. Table 8 shows that all the composites in the present study follow transverse isotropic behavior.

4.2. Strength properties

The material properties are as per Table 9. Composite failure can be characterized as fiber failure or matrix failure, considering our assumption that the interface does not fail. First we will consider loading in the longitudinal or fiber direction. In this case, since fiber failure strain, $e_{f1}^{(+)}$ is higher than matrix failure strain, $e_m^{(+)}$, we can conclude that matrix will govern the failure. So, composite failure will occur at the strain level corresponding to the matrix failure strain, $e_m^{(+)}$. Hence, longitudinal strength of the composite can be predicted from the following relation

$$S_L^{(+)} = E_1 e_m^{(+)} \tag{12}$$

where E_1 is the longitudinal moduli of the composite. This equation gives a good measure of the failure strength for initiation of failure.

Table 4
Longitudinal moduli E_1 for various composites in GPa units. H1···H5 refer to hybrid composites with five different sets of volume fraction as given in Table 1.

Type of composite	Carbon/epoxy	Hybrid composites					Glass/epoxy
		H1	H2	H3	H4	H5	
FE analysis	159	148	125	102	79.0	56.2	44.8
RoHM	159.2	147.7	124.9	102	79.1	56.3	44.8
% Diff (absolute)	0.16	0.16	0.16	0.15	0.14	0.13	0.13

Table 5
Transverse moduli E_2 (GPa) for various composites.

Type of composite	Carbon/epoxy	Hybrid					Glass/epoxy
		H1	H2	H3	H4	H5	
FE analysis	8.77	9.05	9.66	10.33	11.05	11.82	12.21
Modified Halpin Tsai	8.59	8.88	9.52	10.22	11	11.86	12.33
% Diff (absolute)	2.07	1.84	1.47	1.08	0.5	0.37	1.02

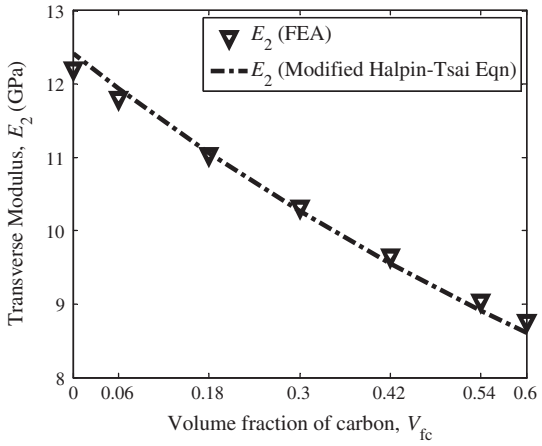

Fig. 5. Variation of E_2 with volume fraction of carbon.

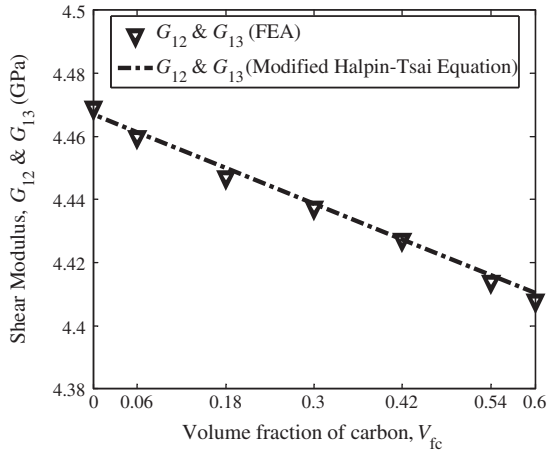

Fig. 7. Variation of G_{12} and G_{13} with volume fraction of carbon.

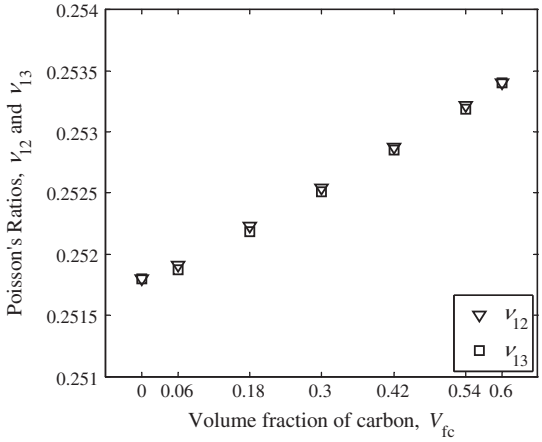

Fig. 6. Variation of ν_{12} and ν_{13} with volume fraction of carbon.

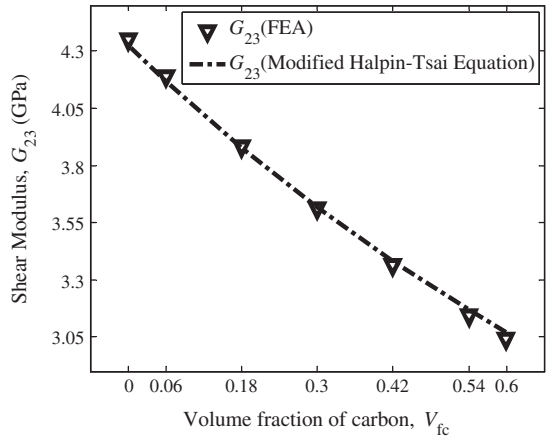

Fig. 8. Variation of G_{23} with volume fraction of carbon.

The results from finite element analysis are plotted against the volume fraction of carbon in Fig. 10. $S_L^{(+)}$ has been calculated from (12) and presented in Table 10. As can be observed, the longitudinal strength varies linearly with volume fraction and can be predicted with reasonable accuracy.

Longitudinal compressive strength of the composites were calculated and plotted with volume fraction of carbon as shown in Fig. 11. Both strengths in the longitudinal direction show a linear dependence with volume fraction. It must be noted, however, that for the compressive strength, no microbuckling of the fiber or instability analysis was performed, and failure was due only to stresses. Detailed micromechanical analysis of failure modes such as microbuckling or kinking can be found in [20,21]. Furthermore, the longitudinal strengths show no variability with fiber location. The linear nature of the plot can be explained from observing (12) which depends on E_1 of the composite. As seen before, E_1

Table 6
Transverse moduli G_{12} (G_{13}) (GPa) for composites.

Type of composite	Carbon/epoxy	Hybrid					Glass/epoxy
		H1	H2	H3	H4	H5	
FE analysis	4.41	4.41	4.43	4.44	4.45	4.46	4.47
Modified Halpin–Tsai	4.41	4.42	4.43	4.44	4.45	4.46	4.47
% Diff (absolute)	0.05	0.04	0.04	0	0.06	0.06	0.05

Table 7
Transverse moduli G_{23} (GPa) for composites.

Type of composite	Carbon/epoxy	Hybrid					Glass/epoxy
		H1	H2	H3	H4	H5	
FE analysis	3.04	3.14	3.36	3.60	3.88	4.19	4.35
Modified Halpin Tsai	3.06	3.16	3.38	3.62	3.88	4.17	4.32
% Diff (absolute)	0.91	0.78	0.59	0.3	0.17	0.63	0.71

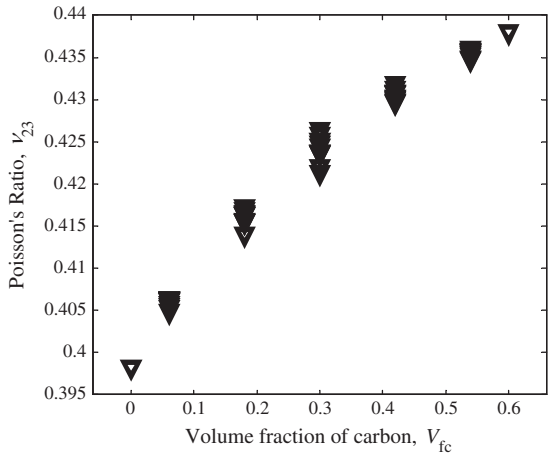

Fig. 9. Variation of v_{23} with volume fraction of carbon.

Table 8
Comparison of G_{23} to test transverse isotropy.

	Specimen	G_{23} (FEA)	$E_2/2\ (1 + v_{23})$	% Difference
Carbon/epoxy		3.04	3.05	0.30
Hybrid composites	H1	3.14	3.15	0.32
	H2	3.36	3.37	0.30
	H3	3.60	3.62	0.55
	H4	3.88	3.90	0.51
	H5	4.19	4.20	0.24
Glass/epoxy		4.35	4.37	0.37

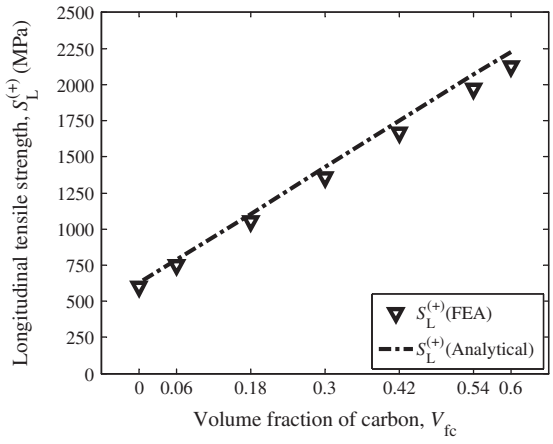

Fig. 10. Variation of $S_L^{(+)}$ with volume fraction of carbon.

Table 9
Strengths of constituent materials [17,19].

	Carbon	Glass	Epoxy
Longitudinal tensile strengths (MPa)	4120	1104	–
Longitudinal compressive strength (MPa)	2990	1104	–
Transverse tensile and compressive strengths (MPa)	298	1104	–
Shear strength (MPa)	1760	460	93
Tensile strength (MPa)	–	–	49
Compressive strength (MPa)	–	–	121

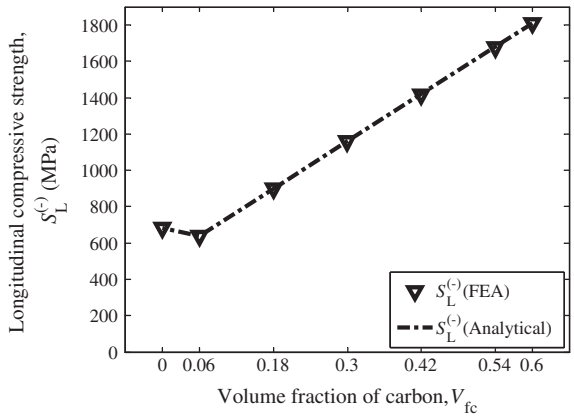

Fig. 11. Variation of $S_L^{(-)}$ with volume fraction of carbon.

has a linear variation with volume fraction of the fiber, hence the strengths follow similar pattern since $e_m^{(+)}$ is a constant for all the samples.

A theory of elasticity analysis for a transverse normal loading of a doubly periodic rectangular array of elastic filaments can be found in [22]. However, a simple analytical model for transverse strength of one reinforcement composite can be found in [14]. The relation has been used to predict the strength of the two phase composites, pure carbon/epoxy and glass/epoxy. When compared with the DMM strength, it has a difference of 15%.

Transverse tensile and compressive strength obtained from DMM approach are plotted in Figs. 12 and 13 with volume fraction of carbon. As observed, transverse strength of the composite reduces when a second reinforcement is added. Hybridization therefore results in lowering the transverse strength. Another very

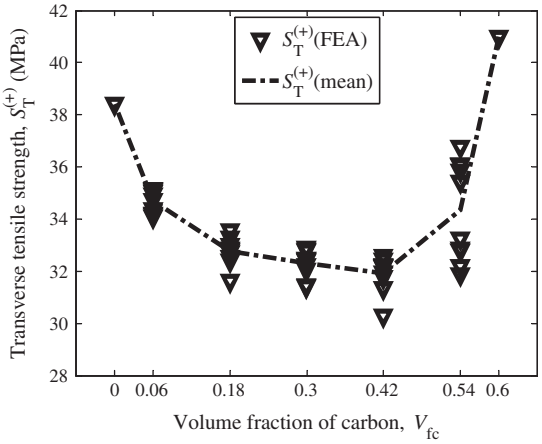

Fig. 12. Variability in $S_T^{(+)}$ with volume fraction of carbon.

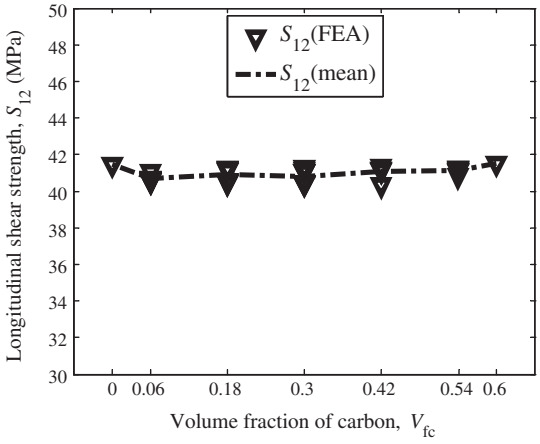

Fig. 14. Variability in S_{12} with volume fraction of carbon.

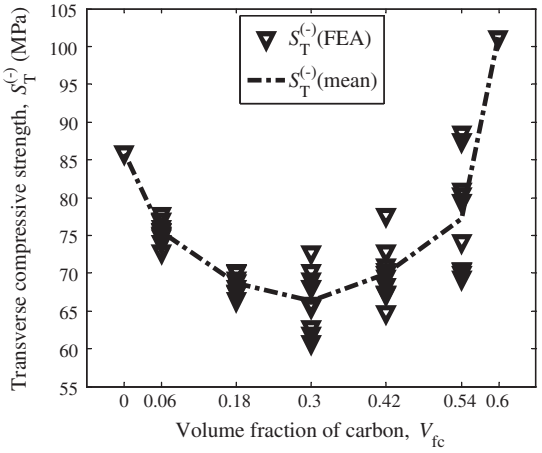

Fig. 13. Variability in $S_T^{(-)}$ with volume fraction of carbon.

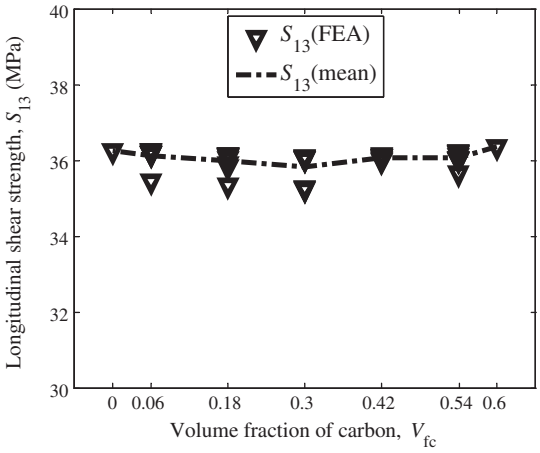

Fig. 15. Variability in S_{13} with volume fraction of carbon.

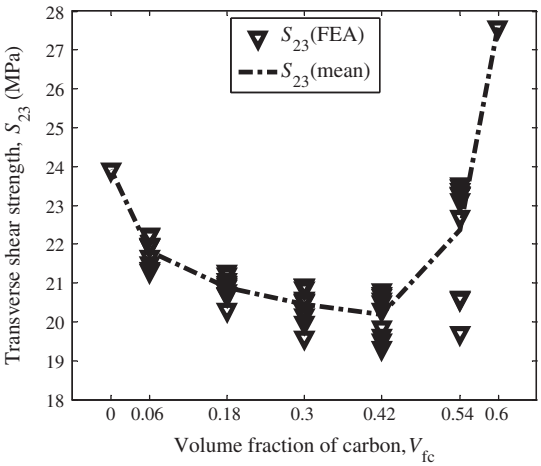

Fig. 16. Variability in S_{23} with volume fraction of carbon.

significant observation is, randomization of fiber locations inside the RVE, brings about significant variability in the strength values.

This observation can be explained as follows. When glass fiber is introduced in a pure carbon/epoxy composite, it behaves as an inclusion in a continuous media and causes local stress concentration. This is because of the transverse modulus of glass which is very high compared to carbon. Hence when 6% glass fiber is introduced in a pure carbon/epoxy composite, we see a larger strength drop, than when 6% carbon fiber is introduced in glass/epoxy composite.

A very similar variation is observed for the transverse compressive strength of the composites. Once again the drop in strength when glass fiber is introduced in carbon/epoxy, is significantly higher than when carbon is introduced into glass/epoxy. Elasticity analysis of an array of elastic filaments subjected to longitudinal shear has been studies by Adam and Doner [23]. Transverse shear strengths S_{12} and S_{13} have been calculated for hybrid composites and presented in Figs. 14 and 15. It is observed that there is negligible variation of transverse shear strengths, owing to the fact that shear strengths are controlled by matrix strength and are essentially same for all the composites.

It should be however noticed that S_{12} and S_{13} are not the same for any composite. This is mostly due to the asymmetric hexagonal arrangement of the fibers in the 1 and 2 directions. Variation of the shear strength S_{23} is also presented for hybrid composites in Fig. 16. Since, S_{23} is an in-plane property in the transverse directions, follows a very similar trend as the transverse tensile and compressive strengths as shown before in Figs. 13 and 14.

It is important to note here that strengths unlike the elastic constants are not equal in 2 and 3 directions. This is owing to the fact that, the RVE is not symmetric about 2 and 3 directions. Although

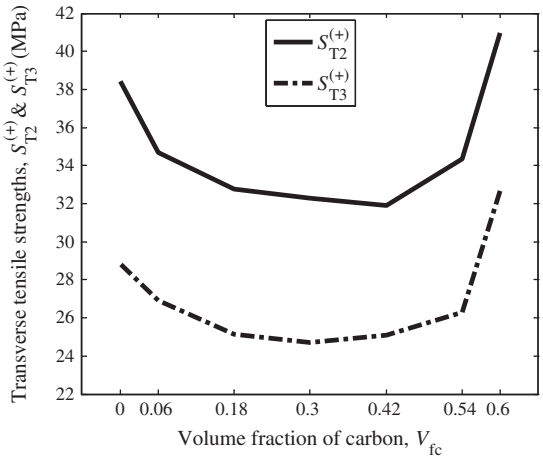

Fig. 17. Comparison of $S_{T2}^{(+)}$ and $S_{T3}^{(+)}$ (mean values) with volume fraction of carbon.

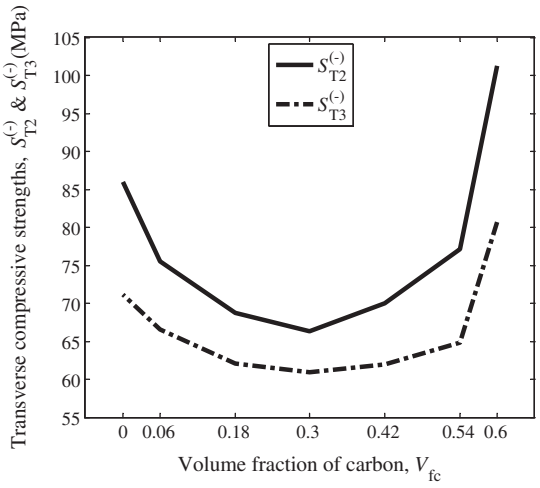

Fig. 18. Comparison of $S_{T2}^{(-)}$ and $S_{T3}^{(-)}$ (mean values) with volume fraction of carbon.

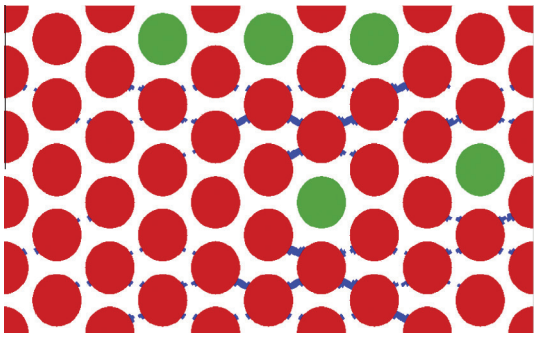

Fig. 20. Failed elements for specimen 5.

average stresses across the RVE were equal, the microstresses inside the RVE are not. A comparison of the variation of $S_T^{(+)}$ and $S_T^{(-)}$ are made for 2 and 3 directions and presented in Figs. 17 and 18 respectively. Here $S_{T2}^{(+)}$, $S_{T2}^{(-)}$ and $S_{T3}^{(+)}$, $S_{T3}^{(-)}$ represent transverse tensile and compressive stresses in the 2 and 3 directions respectively.

In order to explain the effect of hybridization on the transverse strength in more detail, failed elements have been identified in the Figs. 19 and 20. The DMM method of failure is continued till 1% of the volume of the unit cell was failed. Glass fiber is red and carbon green in the above figures. It can be observed that the microstress concentration is always near the region surrounding the glass fibers. This shows that, introduction of glass causes a high local stress concentration owing to its high transverse modulus and thus strength of the composites drop on addition of glass.

All the strength values computed using the present model are presented in Table 11. For the hybrid composite, results for specimen H3 have been provided in this table. As can be observed, both transverse tensile and compressive strengths for hybrid composites are lower than the binary composites. Arithmetic mean, standard deviation and coefficients of variation for strength properties are presented in Table 12. Longitudinal tensile and compressive strengths had no dependence on the fiber location. On the other

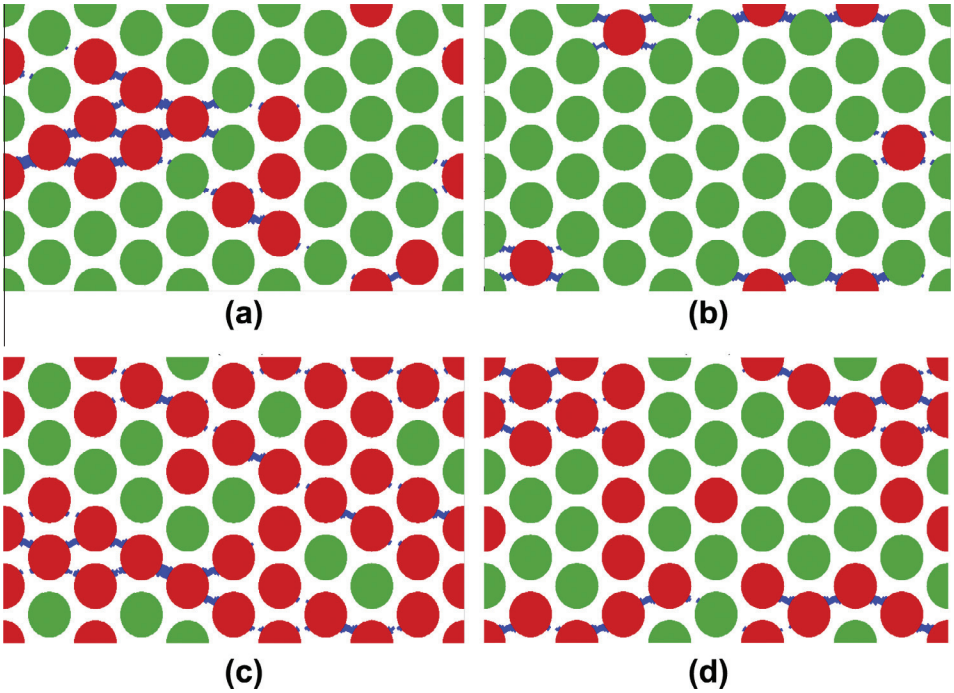

Fig. 19. 19(a–d) Failed elements for random samples for specimens H1, H2, H3 and H4.

Table 10
Longitudinal tensile strength, $S_L^{(+)}$ (MPa) for composites.

Composite	Specimen	FEA	Analytical	% Difference
Carbon/epoxy		2130	2229	4.43
Hybrid	H1	1972	2069	4.67
	H2	1665	1748	4.77
	H3	1360	1428	4.78
	H4	1055	1108	4.79
	H5	750	788	4.81
Glass/epoxy		598	628	4.74

Table 11
Summary of Strength properties for Composites.

Strength	Carbon/epoxy	Glass/epoxy	Hybrid/epoxy
Longitudinal tensile (MPa)	2128	598	1360
Longitudinal compressive (MPa)	1807	684	1158
Transverse tensile (MPa)	41	38	27
Transverse compressive (MPa)	101	86	59
Longitudinal shear, S_{12} (MPa)	42	41	41
Longitudinal shear, S_{13} (MPa)	36	36	36
Transverse shear, S_{23} (MPa)	28	24	20

Table 12
Standard deviation and coefficient of variation for strengths ($\mu, \sigma, \sigma/\mu$ stands for mean, standard deviation and coefficient of variance (%) respectively).

Specimen	$S_L^{(+)}$ (MPa)			$S_L^{(-)}$ (MPa)		
	μ	σ	σ/μ	μ	σ	σ/μ
1	1972	0.45	0.022	1677	0.01	0
2	1666	0.20	0.012	1418	0	0
3	1360	0.14	0.010	1158	0	0
4	1055	0.04	0.003	899	0	0
5	750	0.05	0.006	639	0	0
	$S_T^{(+)}$ (MPa)			$S_T^{(-)}$ (MPa)		
	μ	σ	σ/μ	μ	σ	σ/μ
1	34	1.5	4.4	76	8.5	11.2
2	32	0.5	1.5	67	2.6	3.84
3	32	0.4	1.2	64	3.1	4.80
4	33	0.7	2.1	67	0.9	1.42
5	35	0.5	1.4	75	1.4	1.86

hand, significant variation in the transverse tensile and compressive strengths can be observed as the fibers were randomized. As mentioned before, inclusion of a second fiber in a composite causes stress concentration. This stress concentration depends on the transverse modulus of the fiber introduced.

5. Conclusion

A computational model for hybrid composites using circular fibers in a hexagonal array has been proposed. Some of the parameters that play a key role in studying the hybrid effect on the stiffness and strength properties have been incorporated. The stiffness properties show a smooth linear variation with the change in volume fraction. Also relative location of the different fibers in the unit cell did not affect the stiffness properties by a large amount. The reason for this behavior might be because of the fact that stiffness being a volume averaged quantity, does not depend on the position of the fibers but the effective volume fraction of the reinforcement only. It has been shown that RoHM predicts the longitudinal modulus, longitudinal poisson's ratios and longitudinal shear modulus, with very good accuracy. For predicting the transverse moduli, transverse poisson's ratio and the transverse shear moduli, modified Halpin–Tsai equation has been proposed, that matches the finite element results with reasonable accuracy.

Longitudinal tensile and compressive strengths vary linearly with the volume fraction of the reinforcement, and are dependent on the longitudinal modulus and the least strain to failure of the constituent. All other strengths show variability with the fiber location inside the RVE. This is attributed to the transverse modulus of the introduced fibers to form the hybrid composite, which causes a local stress concentration, resulting in the failure of the neighboring matrix elements.

Experimental data for hybrids has been reviewed by many researchers. It is observed that the rule of mixtures can approximately predict the longitudinal and transverse mechanical properties of unidirectional interply hybrids [1,3,5,6]. This is consistent with the results presented in this paper.

Overall, the objective of the present work was to develop a computational model that is compatible to test hybrid composites with varying volume fraction of reinforcements and study the effect of hybridization on mechanical properties of the composite. Future work in this area would be using similar models to model progressive damage in hybrid composites.

Acknowledgements

The authors sincerely acknowledge the partial support of United States Army Research Office Grant W911NF-08-1-0120 and encouragement of Dr. C.F. Yen of ARL at APG, MD.

References

[1] Chamis CC, Lark RF. Hybrid composites- State-of-the-art review: Analysis, design, application and fabrication. In: 18th Structures, structural dynamics and materials conference. 1977. p. 311–31.
[2] Chou TW, Kelly Anthony. Mechanical properties of composites. Annu Rev Mater Sci 1980;10(1):229–59.
[3] Fu Shao-Yun et al. Hybrid effects on tensile properties of hybrid short-glass-fiber-and short-carbon-fiber-reinforced polypropylene composites. J Mater Sci 2001;36(5):1243–51.
[4] Fu Shao-Yun, Guanshui Xu, Yiu-Wing Mai. On the elastic modulus of hybrid particle/short-fiber/polymer composites. Compos Part B: Eng 2002;33(4):291–9.
[5] Sonparote PW, Lakkad SC. Mechanical properties of carbon/glass fibre reinforced hybrids. Fibre Sci Technol 1982;16(4):309–12.
[6] Venkateshwaran N, Elayaperumal A, Sathiya GK. Prediction of tensile properties of hybrid-natural fiber composites. Compos Part B: Eng 2012;43(2):793–6.
[7] Atiqah A et al. Development of kenaf–glass reinforced unsaturated polyester hybrid composite for structural applications. Compos Part B: Eng 2013.
[8] Jarukumjorn Kasama, Suppakarn Nitinat. Effect of glass fiber hybridization on properties of sisal fiber–polypropylene composites. Compos Part B: Eng 2009;40(7):623–7.
[9] Jawaid M et al. Effect of jute fibre loading on tensile and dynamic mechanical properties of oil palm epoxy composites. Compos Part B: Eng 2013;45(1):619–24.
[10] Ramesh M, Palanikumar K, Hemachandra Reddy K. Mechanical property evaluation of sisal–jute–glass fiber reinforced polyester composites. Compos Part B: Eng 2012.
[11] Boopalan M, Niranjanaa M, Umapathy MJ. Study on the mechanical properties and thermal properties of jute and banana fiber reinforced epoxy hybrid composites. Compos Part B: Eng 2013.
[12] Mirbagheri Jamal et al. Prediction of the elastic modulus of wood flour/kenaf fibre/polypropylene hybrid composites. Iranian Polym J 2007;16(4):271–8.
[13] Karkkainen Ryan L, Sankar Bhavani V, Tzeng Jerome T. Strength prediction of multi-layer plain weave textile composites using the direct micromechanics method. Compos Part B: Eng 2007;38(7):924–32.
[14] Gibson Ronald F. Principles of composite material mechanics. 3rd ed. CRC PressI Llc; 2011.
[15] Zhu H, Sankar BV, Marrey RV. Evaluation of failure criteria for fiber composites using finite element micromechanics. J Compos Mater 1998;32(8):766–82.
[16] Sun CT, Vaidya RS. Prediction of composite properties from a representative oopalvolume element. Compos Sci Technol 1996;56(2):171–9.
[17] Choi Sukjoo, Sankar Bhavani V. Micromechanical analysis of composite laminates at cryogenic temperatures. J Compos Mater 2006;40(12):1077–91.

[18] Hashin Z. Failure criteria for unidirectional fiber composites. J Appl Mech June 1980;47:329–34.
[19] Stamblewski, Christopher, Sankar Bhavani V, Zenkert Dan. Analysis of three-dimensional quadratic failure criteria for thick composites using the direct micromechanics method. J Compos Mater 2008;42(7):635–54.
[20] Schultheisz Carl R, Waas Anthony M. Compressive failure of composites, part I: testing and micromechanical theories. Progr Aerospace Sci 1996;32(1):1–42.
[21] Waas Anthony M, Schultheisz Carl R. Compressive failure of composites, part II: experimental studies. Progr Aerospace Sci 1996;32(1):43–78.
[22] Adams Donald F, Doner Douglas R. Transverse normal loading of a unidirectional composite. J Compos Mater 1967;1(2):152–64.
[23] Adams Donald F, Doner Douglas R. Longitudinal shear loading of a unidirectional composite. J Compos Mater 1967;1(1):4–17.